Pergamon

Geochimica et Cosmochimica Acta, Vol. 66, No. 22, pp. 3971–3986, 2002

0016-7037/02 $22.00 + .00

PII S0016-7037(02)00963-8

Phase relations in the CH_4-H_2O-NaCl system at 2 kbar, 300 to 600°C as determined using synthetic fluid inclusions

WILLIAM M LAMB,* CHRISTOPHER J. MCSHANE, and ROBERT K. POPP
Department of Geology and Geophysics, Texas A&M University, College Station, TX 77843-3115

(*Received June* 13, 2001; *accepted in revised form May* 20, 2002)

Abstract—Synthesis of fluid inclusions in the CH_4-H_2O-NaCl system was accomplished by subjecting fractured quartz or fluorite, along with known quantities of CH_4, H_2O, and NaCl, to a pressure of 2 kbar and temperatures of 300, 400, 500, or 600°C, in sealed Au capsules. Under the elevated P-T conditions, some of the fractures healed, trapping fluids as inclusions. Microthermometric measurements conducted on the fluid inclusions show that at 2 kbar and 400 to 600°C, there are very broad regions of fluid unmixing in the CH_4-H_2O-NaCl system. For those bulk fluid compositions that lie in the two-phase (i.e., immiscible fluids) field, the high-density phase is enriched in NaCl, whereas the low-density phase is enriched in CH_4. For any given bulk composition, the degree of NaCl enrichment in the high-density phase increases, whereas the degree of CH_4 enrichment in the low-density phase decreases, as temperature increases from 400 to 600°C. Our experimental constraints on the size of the two-phase field are generally consistent with results generated using the equation-of-state GEOFLUIDS (available at http://geotherm.ucsd.edu/geofluids/). However, when comparing the compositions of coexisting immiscible fluids, as determined experimentally vs. calculated using GEOFLUIDS, we find that some relatively small but probably significant differences exist between our experiments and this equation of state.

1. INTRODUCTION

Fluids play an important role in many geologic processes, such as the formation of ore deposits, hydrocarbon migration, volcanism, melting at midocean ridges and convergent margins, and many metamorphic processes (Roedder, 1979, 1984; Emery and Robinson, 1993; Hedenquist and Lowenstern, 1994, Carroll and Holloway, 1994; Hirth and Kohlstedt, 1996). In particular, species in C-O-H-salt systems are the most frequently encountered species in natural fluids (Roedder, 1972, 1979, 1984; Crawford, 1981).

In this study, the experimental and analytical techniques described by Lamb et al. (1996) were used to synthesize and analyze CH_4-H_2O-NaCl fluid inclusions at 2 kbar and 300, 400, 500, and 600°C. The fluid compositions of interest to this study occur within the C-O-H-NaCl system, which defines the composition of fluids in a wide range of geologic environments. Whereas CH_4-rich fluids clearly have a more restricted occurrence than H_2O-NaCl or CO_2-H_2O-NaCl fluids, methane-bearing fluids have been reported from a variety of geologic environments, including high-grade diagenetic to very low-grade metamorphic zones of the central Alps (Mullis et al., 1994) and central Appalachians (Kisch and van den Kerkhof, 1991). Rocks from higher-grade contact and regional metamorphic settings also contain methane-bearing fluids (Kisch and van den Kerkhof, 1991; Heinrich, 1993), as do igneous rocks such as the Skaergaard intrusion (Larsen et al., 1992) and some oceanic gabbros (Kelley, 1996). The results of this study should have application to understanding CH_4-rich fluids from the higher temperature environments. In addition, the results should provide input for refining equation-of-state models in the larger C-O-H-NaCl system (e.g., Duan et al., 1992a, 1992b, 1995).

* Author to whom correspondence should be addressed (lamb@geo.tamu.edu).

It is well-documented that synthetic fluid inclusions can be used to determine P-V-T properties and phase relations of fluids and to understand the behavior of natural fluid inclusions. Shelton and Orville (1980) first documented that synthetic fluid inclusions can be employed to trap representative samples of fluids at elevated temperatures and pressures. Similar techniques have been used to determine molar volumes as a function of P and T and to determine phase relations for a number of fluids and fluid mixtures. Studies of this type include work with pure fluids, such as H_2O (Bodnar and Sterner, 1985; Zhang and Frantz, 1987), as well as binary and ternary H_2O-salt systems such as H_2O-NaCl (Bodnar et al., 1985; Zhang and Frantz, 1987), H_2O-KCl (Zhang and Frantz, 1987; Sterner et al., 1988), and H_2O-KCl-NaCl (Sterner et al., 1988). Binary fluid systems such as H_2O-CO_2 (Sterner and Bodnar, 1991), and H_2O-CH_4 (Zhang and Frantz, 1992), as well as ternary systems involving salts such as H_2O-CO_2-NaCl (Frantz et al., 1992; Schmidt et al., 1995; Schmidt and Bodnar, 2000) have also been investigated using synthetic fluid inclusions. These studies have generally produced data in agreement with those obtained using other techniques (e.g., Bodnar and Sterner, 1985; Zhang and Frantz, 1987; Brown and Lamb, 1989; Sterner and Bodnar, 1991).

Lamb et al. (1996) used synthetic fluid inclusions to determine the phase relations in the CH_4-H_2O-NaCl system at 1 kbar and temperatures in the range 400 to 600°C. Microscopic examination of the fluid inclusions, combined with microthermometric measurements, provided the data necessary to locate the position of the solvus between the one-phase and two-phase fields and to define the compositions of the coexisting fluids in the two-phase field. In the study described here, the range of conditions has been expanded to higher pressure and slightly lower temperatures. Phase relations in the CH_4-H_2O-NaCl system were determined using synthetic fluid inclusions produced

at 2 kbar and 300, 400, 500, and 600°C. Our results are complimentary to and extend the pressure, temperature, or compositional range covered by previous experimental work (Krader, 1985; Lamb et al., 1996).

2. MATERIAL AND METHODS

Natural quartz and synthetic fluorite (obtained from SOREM, zone artisanale, Route de Nay, 64110 –Uzos, France) crystals were used to host the fluid inclusions. These crystals were cut into prisms ($\sim 2 \times 3 \times 10$–20 mm). The prisms were cleaned by rinsing first in concentrated HCl and then acetone, followed by several rinses in distilled-deionized H_2O. The quartz prisms were heated to 1000°C for 12 h in an effort to eliminate any preexisting submicroscopic fluid inclusions. Because fluorite has a tendency to shatter at higher temperatures, the fluorite was only heated to 300°C. All prisms were subsequently heated to 300 to 325°C and immediately immersed in distilled, deionized water at room temperature. The thermal shock of cooling produced small fractures that provided conduits for trapping the fluid.

The fractured prisms were dried overnight at ~130°C and placed in an annealed Au capsule (4.75 mm OD × 4.50 mm ID × 76 mm). Known amounts of H_2O + NaCl solutions of various molalities were placed in the capsule along with the prism. A small amount of quartz or fluorite powder was added in the capsule to promote fracture healing.

After the Au capsule was attached to the gas-loading apparatus shown in Figure 1 (design based on Frantz et al., 1989), the H_2O + NaCl solution was frozen by applying a liquid nitrogen bath to the lower end of the capsule. A vacuum pump was used to remove all noncondensable species from the capsule. After the capsule was evacuated, it was isolated from the vacuum pump by closing valve C (refer to Fig. 1 for apparatus layout). Methane was transferred into the shaded portion of the vacuum line between valves A and B, the volume of which had been determined previously. (Given that the volume of methane is known, it is possible to calculate the number of moles of methane from the Ideal Gas Law at a given pressure and temperature.) The methane was then condensed into the Au capsule, which was still immersed in liquid nitrogen, by opening valve B. The capsule was cold welded as it was cut from the apparatus with a pinch-off device. The Au capsule, which contained known amounts of CH_4, H_2O, and NaCl was electric arc welded while still immersed in liquid nitrogen.

During the transfer of methane via condensation into the Au capsule, some of the gas remained in the apparatus, because methane has significant vapor pressure at liquid nitrogen temperatures. It is possible to calculate the number of moles of this residual methane as described in detail by Lamb et al. (1996).

The Au capsules, containing quartz or fluorite and known amounts of CH_4-H_2O-NaCl, were placed in horizontally mounted, cold-seal hydrothermal vessels with methane used as the pressure medium. Temperatures were measured by means of sheathed chromel-alumel thermocouples. Pressure within the vessel was measured by a Heise bourdon gauge that was factory calibrated and set to read 0 at atmospheric pressure.

To avoid the formation of inclusions during the runup to the desired experimental temperatures, the furnaces were preheated. Each vessel was heated to within 10°C of the final desired temperature within 10 min after it was inserted into the furnace. The experimental T and P were maintained for 4 to 33 d. In general, lower temperatures required longer residence time in the vessels to allow more time for fracture healing. At the end of each experiment, the vessels were cooled to <75°C within 10 min using a stream of compressed air. The capsules were removed from the vessels and weighed, punctured to release the gas, and weighed again, placed in a drying oven overnight to remove the H_2O, and weighed a final time. As discussed in detail below, the weights of gas released on puncturing and H_2O lost during drying was used to confirm that the compositions of the fluids in the capsules did not change during the experiment.

2.1. Microthermometry: Procedures and Results

The prisms were cleaned and polished after inclusion synthesis. A Fluid Inc. modified U.S.G.S. gas-flow heating/freezing stage was used to perform microthermometric measurements. The thermocouple used for microthermometric measurements was calibrated against the CO_2 triple point and H_2O (ice) melting point. Homogenization temperatures were measured, as well as melting temperatures of NaCl daughter crystals, if present. Fluid inclusions used for measurements ranged in size from 4 to 34 μm in length. The most common size was between 10 and 15 μm. The results of microthermometric measurements are given in Table 1.

Fluorite was used as the host material for the experiments performed at 300°C (the letter F follows the sample numbers using fluorite in Table 1). Previous experience (e.g., Lamb et al., 1996) indicates that as the experimental temperature decreases, the size and quantity of inclusions also decrease. Thus, the duration of experiments performed at 400°C is generally longer than for those experiments performed at higher temperatures to produce more inclusions suitable for microthermometric measurements. We used fluorite for lower temperature experiments (300°C) because of the suggestion that fracture healing in fluorite was more rapid than in quartz. Presumably, the relatively high solubility of fluorite would facilitate the healing of fractures, therefore, forming larger and more abundant inclusions (J. Dubessy, pers. comm. with Robert Popp). Preparing the fluorite for microthermometry required greater care because of the tendency of fluorite to cleave when cutting and polishing.

Seven experiments were performed at 300°C, but only four samples produced fluid inclusions that were suitable for microthermometric measurements (experiments 105F, 108F, 111F, and 113F; Table 1). These four experiments produced fluid inclusions that were generally small and few in number.

3. POSSIBLE CHANGES IN FLUID COMPOSITIONS DURING AN EXPERIMENT

For the results of the experiments to be accurate, it is important that the amounts of the gases initially loaded into the capsules do not change during the experiments. At pressures and temperatures relevant to this study, additional fluid species such as CO_2, CO, and H_2 may form in significant quantities. Changes could occur in a closed system, possibly driven by reactions between CH_4 and H_2O to produce small amounts of CO_2, CO, and H_2. Alternatively, the transfer of matter between the interior and exterior of the capsule (e.g., diffusion of H_2 through the walls of the gold capsule) could drive changes in the composition of the fluid within the capsule.

3.1. Closed-System Changes

Zhang and Frantz (1992) investigated the possibility that C-O-H fluid species, other than CH_4 and H_2O, formed during the synthesis of fluid inclusions. They analyzed the gas in quenched capsules by gas chromatography and demonstrated that the amounts of H_2O and CH_4 present in the capsule after each experiment were equivalent, within analytical uncertainty, to the amounts originally loaded into the capsules. Furthermore, the P-T location of the liquid-vapor curve in the CH_4-H_2O system, based on their microthermometric measurements, compares favorably with the experimental results of Welsch (1973).

Lamb et al. (1996) used the computer program CALCOH (Lamb and Valley, 1984, 1985; Lamb et al., 1987) to calculate amounts of fluid species other than CH_4 and H_2O that may be present in the capsules during experiments in the CH_4 + H_2O + NaCl system at 1 kbar. These calculations indicate that, for a wide range of carbon activities, the amounts of CO_2, CO, and H_2 are negligible.

Thus, our calculations agree with the results of Zhang and Frantz (1992) that demonstrated that fluid inclusions containing

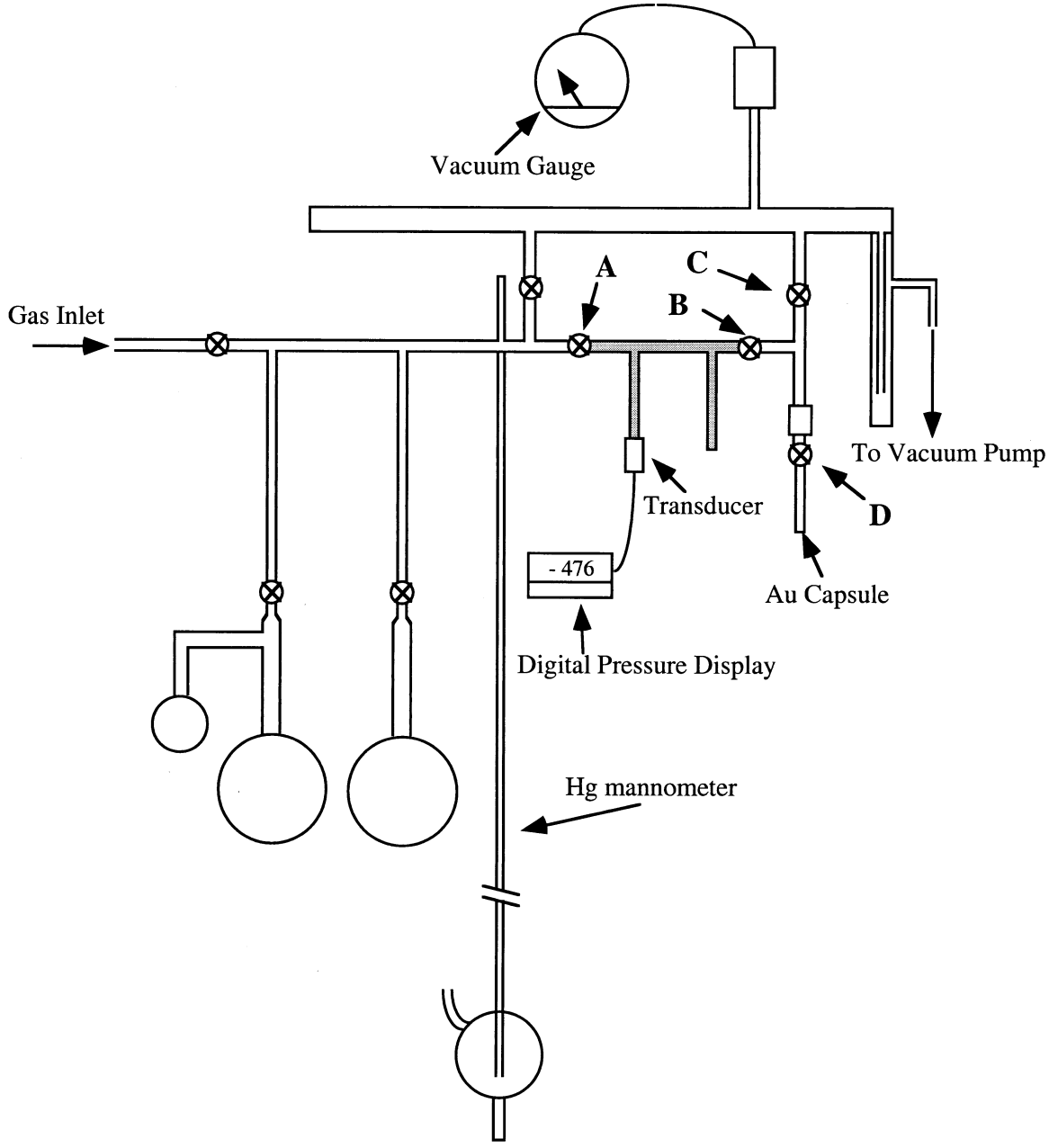

Fig. 1. Gas-loading apparatus used to transfer methane or other gases into noble metal capsules. This apparatus is modified from the design of Frantz et al. (1989) and, unless otherwise indicated, is constructed from glass tubing. Gas at room temperature is transferred into the shaded portion of the apparatus. The volume of this portion of the apparatus (between valves labeled A and B) has been previously determined. Thus, the number of moles of gas can be calculated using the ideal gas law as the temperature, pressure, and volume are known quantities. This gas is then transferred into the Au capsule (see text).

essentially binary CH_4-H_2O mixtures may be produced experimentally. Our own experimental results indicate that addition of NaCl to this system does not alter this conclusion (Lamb et al., 1996).

3.2. Changes in Fluid Speciation due to H-Diffusion

After each experiment, the masses of gas and water in the capsule were measured as follows: The cleaned, dried capsule was weighed, punctured carefully with a stainless steel needle to release the gas, and then reweighed. The difference between the two weights is inferred to represent loss of gas phase from the capsule. The capsule was then placed in a drying oven overnight at ~130°C to remove the water and weighed a final time. Figure 2 shows the results of these measurements. Plotted on the x-axis is the difference between the weight of the CH_4 loaded into the capsules and the weight of the gas present after

Table 1. Results of experiments performed at 2 kbar.

Experimental			Weight % Bulk Composition			Mole % Bulk Composition			Homogenization Temperatures	NaCl Melting Temperatures		Wt% NaCl in liquid	Mole% NaCl in liquid
Run #	Temp. (°C)	Duration Days	NaCl	H_2O	CH_4	NaCl	H_2O	CH_4	(°C)	Low, °C	High, °C	Sterner et al. (1988)*	
105F	300	19	8.92	76.32	14.76	2.87	79.77	17.36	301				
108F	300	20	16.16	69.12	14.72	5.49	76.25	18.26	300				
111F	300	33	0.00	94.51	5.49	0.00	93.87	6.13	298.5–300.1				
113F	300	33	5.19	88.76	6.05	1.64	91.35	7.01	300.5–300.7				
77	400	15	9.66	82.67	7.67	3.16	87.69	9.15	354.7–399				
78	400	15	7.84	67.04	25.13	2.47	68.62	28.91	>400–410				
79	400	15	6.02	51.53	42.45	1.83	50.97	47.20					
80	400	21	3.50	29.96	66.54	1.02	28.30	70.68	>400	279.0	291	37.5	15.6
93	400	17	17.67	75.59	6.74	6.14	85.31	8.55	405.0				
94	400	17	14.51	62.08	23.40	4.81	66.85	28.33	400–418				
95	400	17	11.23	48.04	40.73	3.56	49.38	47.07	405–412	14.5	15.1	26.3	9.9
96	400	17	6.71	28.70	64.60	2.00	27.75	70.25		361.2	375.5	44.9	20.0
101	400	18	5.08	86.89	8.03	1.60	89.13	9.27	368.5–373.3				
102	400	18	4.61	78.92	16.47	1.44	79.83	18.74	396–402				
103	400	18	4.07	69.64	26.29	1.25	69.31	29.44	400.0				
104	400	18	3.55	60.74	35.71	1.07	59.54	39.38	400–402				
141	400	20	2.62	89.63	7.75	0.81	90.39	8.79	370–375				
142	400	20	18.30	78.28	3.43	6.42	89.19	4.39	397–406				
146	400	24	10.34	88.43	1.23	3.42	95.08	1.49	269.0–284.2				
66	500	10	17.69	75.68	6.64	6.15	85.43	8.42	450–460				
67	500	10	16.25	69.50	14.25	5.53	76.77	17.70	500				
68	500	10	14.59	62.41	23.01	4.84	67.27	27.88		226.1	228.1	33.4	13.4
73	500	6	2.61	89.18	8.21	0.81	89.89	9.30	365.8				
74	500	6	2.36	80.78	16.86	0.72	80.41	18.87	380–384(C)				
76	500	6	1.82	62.10	36.09	0.54	60.16	39.30		176	177	30.8	12.0
85	500	10	13.57	58.06	28.37	4.44	61.68	33.88		288	288.6	37.3	15.5
86	500	10	10.95	46.83	42.22	3.45	47.95	48.60		398	403.1	47.8	22.0
87	500	10	8.96	38.33	52.71	2.75	38.19	59.06		468	480	57.1	29.1
88	500	10	7.02	30.02	62.97	2.10	29.15	68.75	>510	506.8	506.8	60.7	32.2
89	500	12	5.09	87.13	7.78	1.61	89.41	8.98	376–383				
90	500	12	4.64	79.44	15.92	1.45	80.43	18.12	422–425 (V)				
91	500	12	4.13	70.74	25.13	1.27	70.55	28.18	448–512				
92	500	12	3.53	60.47	36.00	1.07	59.26	39.67	500–514	226.0	228.1	33.4	13.4
145	500	20	9.46	80.93	9.61	3.08	85.50	11.42	420–434.5				
81	600	5	9.81	83.94	6.25	3.22	89.31	7.48	451–458				
82	600	5	9.64	82.49	7.87	3.15	87.47	9.39	460–462				
83	600	5	7.89	67.48	24.64	2.49	69.13	28.38	607	372	406.6	48.2	22.3
84	600	5	6.88	58.90	34.21	2.13	59.20	38.66		441.4	463.4	54.9	27.3
97	600	5	5.12	87.62	7.26	1.62	89.99	8.39	397–404				
98	600	5	4.62	79.04	16.34	1.44	79.97	18.59	450 (V)				
99	600	5	4.10	70.21	25.69	1.26	69.95	28.79		312.7	342.5	41.7	18.1
100	600	5	3.61	61.72	34.67	1.09	60.61	38.30		432.9	452.5	53.6	26.2
139	600	11	17.05	72.93	10.02	5.87	81.53	12.60	600(C) & ≥616				
140	600	11	1.85	63.22	34.93	0.55	61.33	38.12		330	344	41.9	18.1
143	600	4	8.85	75.71	15.44	2.84	79.03	18.13	>585 (V)				
144	600	4	14.86	63.59	21.55	4.95	68.82	26.23		385	403.5	47.8	22.0

*See Text

the experiment. The y-axis in Figure 2 shows the difference between the weight of the H_2O loaded into the capsule and the weight of the H_2O lost during overnight drying. In most cases, weight changes are <0.5 mg and are within the uncertainty of this technique. In most experiments at 300, 400, and 500°C, the change in the weight of the gas indicates that more gas was loaded into the capsule than was released when the capsule was punctured (small negative shift in the x-direction in Fig. 2). This relatively small change in the weight of the gas is consistent with some residual methane remaining in the capsule after puncturing.

For sample 146, H_2O was expelled during the puncturing process, and, therefore, the weights are not plotted in Figure 2. Also, samples 105F and 108F yielded relatively large changes in weight and are not plotted in Figure 2. Examination of the fluid inclusions from these samples indicates that these capsules maintained their integrity throughout most of the experiment, although loss of integrity may have occurred during depressurization and cooling, or H_2O lost during puncturing may have escaped notice. Thus, we have included the microthermometric results from experiments 105F and 108F in this study.

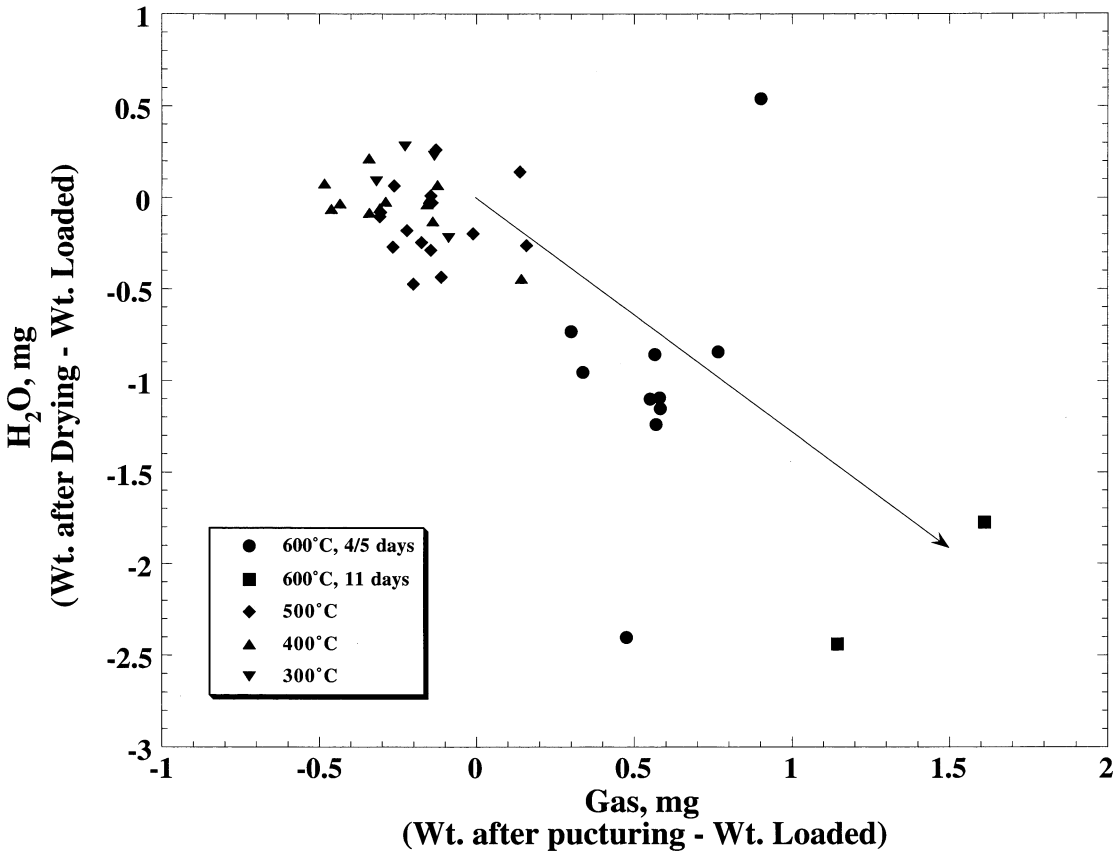

Fig. 2. Changes in the weight of gas and H_2O during each experiment. The x-axis indicates the difference between weight of the gas released on puncturing and the weight of the CH_4 originally loaded. The difference between the weight of the H_2O driven off during drying and the weight originally loaded is plotted on the y-axis. The arrow shows the predicted change in the weights of gas and H_2O caused by H_2 loss with formation of CO_2 at the expense of CH_4 and H_2O. These results suggest that H_2 diffusion was a potential problem for relatively long-duration experiments (11 d) performed at 600°C.

Lamb et al. (1996) also determined the amounts of gas and H_2O present in their capsules using the same puncturing and drying technique described above. For their experiments performed at 1 kbar, they found that when Ar was used as a pressure medium, the weight of the gas in the capsule increased, while the weight of H_2O decreased, during the course of the experiment. These results indicated that loss of H_2 by diffusion through the Au capsule had occurred. Loss of hydrogen from the Au capsules during experiments would drive the following equilibrium to the right:

$$CH_4 + 2H_2O = CO_2 + 4H_2 \quad (1)$$

consuming CH_4 and H_2O and generating CO_2. Even though CO_2 replaces CH_4 in a 1 : 1 molar ratio, the larger molecular weight of CO_2 (44 vs. 16 g/mol) increases the mass of the gas mixture that is present in the capsule after the experiment. The increase in the weight of the gas, due to production of CO_2, more than compensates for the H_2 loss during the experiment.

Lamb et al. (1996) were able to avoid the problem of hydrogen diffusion primarily by employing a CH_4 pressure medium but also by limiting the time of the 600°C experiments. The inherently higher fH_2 of the CH_4 pressure medium, compared with the Ar pressure medium, decreases the H_2 loss through the Au capsule wall. A CH_4 pressure medium was used in the hydrothermal vessels for experiments performed at 2 kbars for this study.

In addition to postexperimental weight changes for gold capsules, Figure 2 also indicates weight change that would result if H-diffusion were responsible for the weight loss (arrow). Weight changes for experiments at 300, 400, and 500°C are all $<\pm 10\%$ of the original loaded value. In most cases, these changes in weight are consistent with the presence of residual methane remaining in the capsule after puncturing and are not consistent with the formation of CO_2 via Eqn. 1. Furthermore, because the weight of the gas did not increase during experiments performed at temperatures <600°C, we conclude that there is neither evidence of CO_2 production nor any indication that H_2 diffused into the capsule.

The changes in weight of both H_2O and gas for those experiments performed at 600°C are somewhat larger than for experiments performed at lower temperatures. In particular, samples that were at elevated temperatures and pressures for 11 d at 600°C yielded the largest weight changes, which are largely consistent with H-diffusion-induced changes in mass

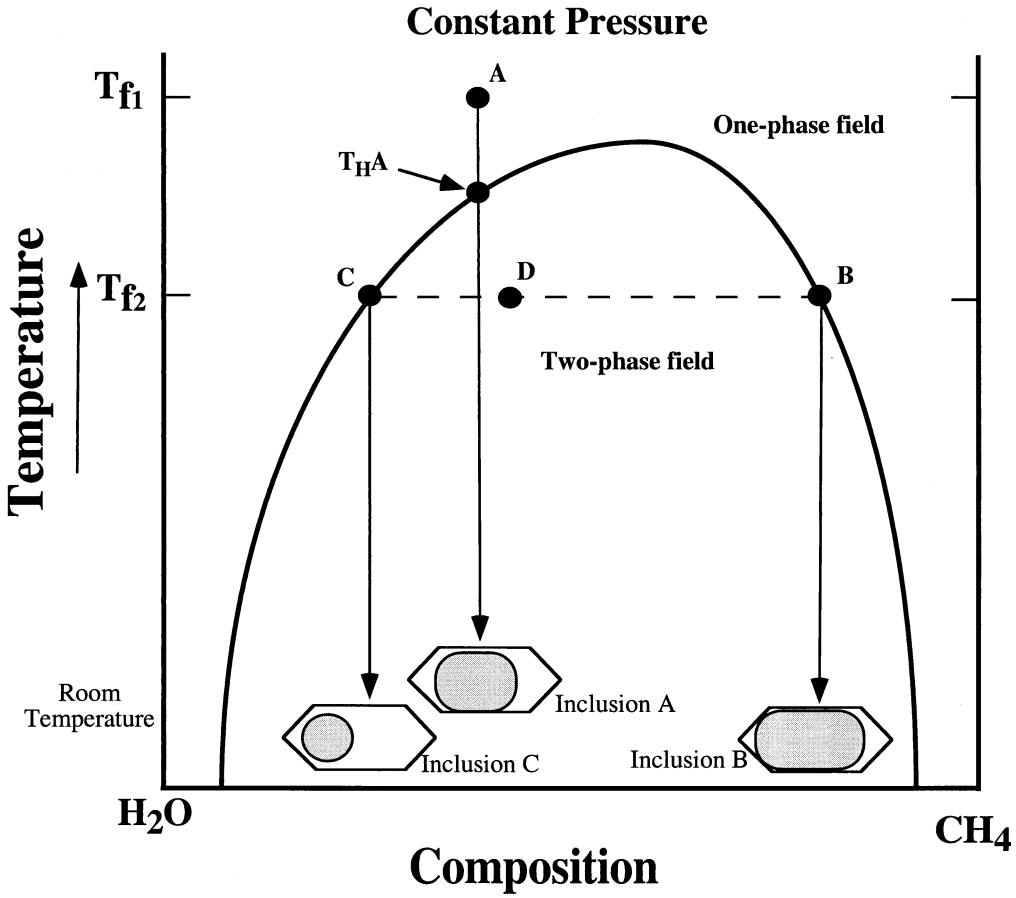

Fig. 3. Phase diagram illustrating the difference between fluid inclusions trapped in the one- and two-phase fields for the binary CH_4-H_2O system. Inclusions trapped in the one-phase field (e.g., point A) will contain a CH_4-rich vapor bubble and an H_2O-rich liquid component on cooling to room temperature (inclusion A). For a bulk composition in the two-phase field (point D), fluids with two different compositions (C and B) will form from immiscible fluids. One set of inclusions is CH_4-rich and, therefore, at room temperature will contain a relatively large vapor bubble (e.g., inclusion B). The coexisting set of inclusions will be rich in H_2O. At room temperature, these H_2O-rich inclusions will contain a relatively small vapor bubble (e.g., inclusion C). The ternary CH_4-H_2O-NaCl system behaves in a similar manner such that inclusions trapped in the one-phase field should all have the same ratio of CH_4-rich vapor to H_2O-rich liquid (similar to point A in this binary diagram), whereas a bulk composition in the two-phase field will yield two sets of fluid inclusions with different liquid-to-vapor ratios (similar to points B and C in this binary diagram). These two sets of inclusions will also have different salinities, as NaCl will partition into the H_2O-rich fluid (see text).

(see experiments 139 and 140 and Fig. 2). Consequently, data from these two experiments are not included in subsequent discussions of phase relations inferred from microthermometric measurements.

It might be argued that even those experiments with durations of 4 to 5 d at 600°C underwent changes in weights of both gas and H_2O that may be consistent with production of CO_2 via Eqn. 1. However, these weight changes (for 600°C, 2 kbar experiments lasting 4–5 d) are small relative to the uncertainty involved in determining the change in weights of both the gas and H_2O. In one case with a relatively large change in the weight of both gas and H_2O (experiment #81), the weight of the gas changed by ~25% and the weight of the H_2O changed by ~4%. If these changes in weight were driven entirely by H_2 loss via Eqn. 1, then a ~25% increase in the weight of the gas would occur if the original composition (3.21 mol.% NaCl, 89.31 mol.% H_2O, and 7.48 mol.% CH_4) changed to ~3.29 mol.% NaCl, 89.07 mol.% H_2O, 6.55 mol.% CH_4, and 1.49 mol.% CO_2. Thus, fluid inclusions in the experiment that yielded one of the largest percentage changes in weight of the gas would contain only ~1.5 mol.% CO_2. This, of course, assumes these weight changes are due totally to the presence of CO_2. Furthermore, Lamb et al. (1996) observed similar weight changes for some of their experiments performed at 1 kbar. However, Lamb et al. (1996) then performed shorter-term experiments with nearly identical starting compositions, and these experiments resulted in insignificant weight changes and thus showed little or no evidence of CO_2 production. These two sets of experiments (original experiments with significant weight changes vs. shorter-term experiments) produced inclusions with essentially identical fluid compositions, as inferred from microthermometric measurements (Lamb et al., 1996). Therefore, we conclude that some of the largest weight changes observed (e.g., ≈ 0.5-mg change in the weight of the gas and

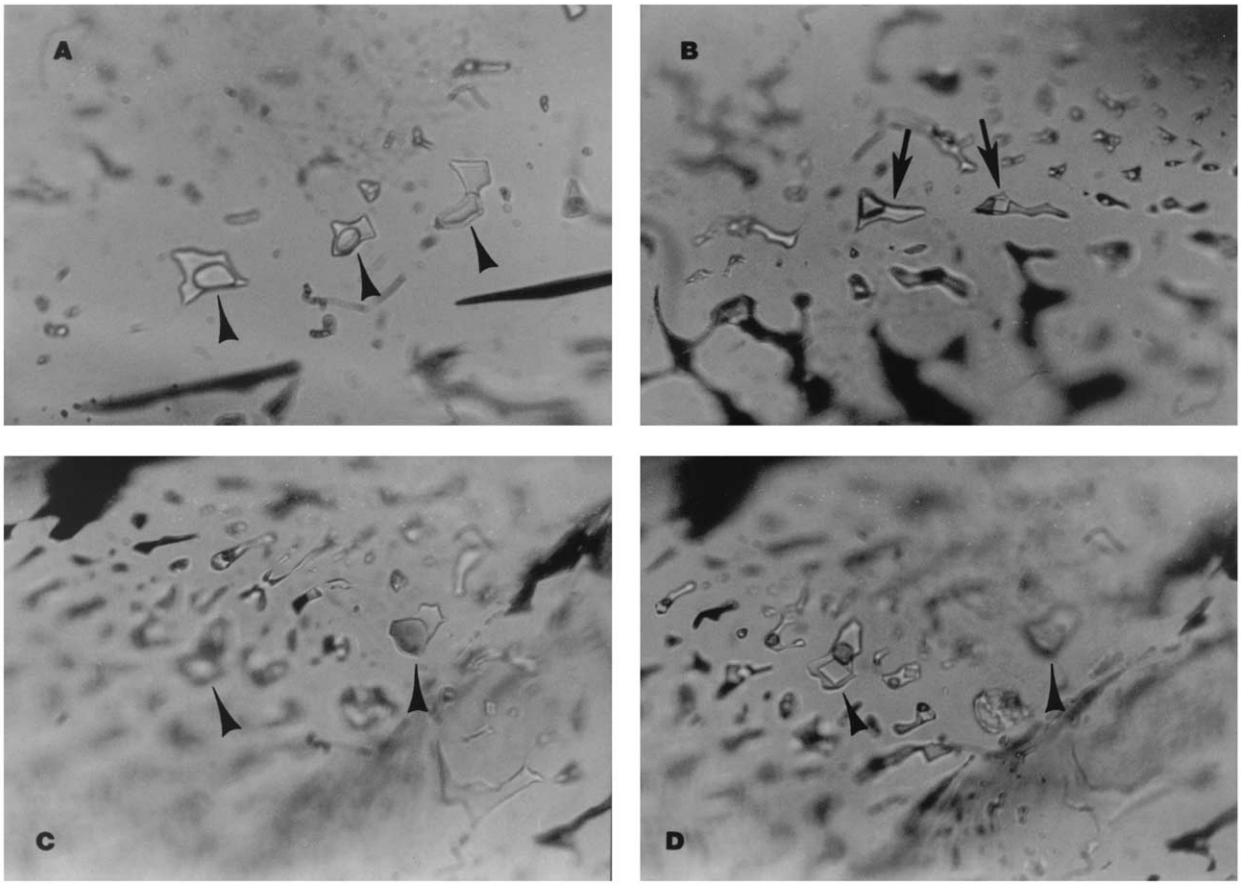

Fig. 4. These four photomicrographs illustrate some of the types of fluid inclusions produced in our experiments performed at 2 kbar (the width of photograph A corresponds to 0.2 mm, whereas the widths of B, C, and D correspond to 0.25 mm). If the bulk fluid composition was in the one-phase field, then a single population of inclusions is produced, as illustrated by the trail of inclusions shown in A. In this case, all inclusions have identical ratios of liquid to vapor, as illustrated by three inclusions (arrows). The other photomicrographs illustrate the results of experiments in which the bulk fluid composition was determined to lie within the two-phase field. In some cases, individual trails contain either H_2O+NaCl-rich or CH_4-rich fluid inclusions. In other cases, both types of inclusions, H_2O+NaCl-rich and CH_4-rich, are in close proximity (photomicrographs B, C, and D). In photomicrograph B, the inclusion on the left (arrow) contains a relatively large vapor bubble, while the inclusion on the right (arrow) contains a relatively small vapor bubble and a single NaCl crystal. C and D are photomicrographs of the same region of quartz (the arrows in C point to the same fluid inclusions as the arrows in D) but were taken at different planes of focus. Photomicrograph C shows an inclusion with a relatively large vapor bubble (arrow on right), whereas the inclusion in D (arrow on left) contains a relatively small vapor bubble and a single NaCl crystal. Observations such as these, combined with microthermometry, were used to determine if bulk compositions were within the one- or two-phase fields.

≈ -1-mg change in the weight of the H_2O), which might indicate the presence of CO_2, actually have insignificant effects on the results of this study.

4. DETERMINATION OF ONE-PHASE VS. TWO-PHASE REGIONS

Figure 3 is a T-X diagram (P = constant) that illustrates, in a schematic fashion, the phase relations associated with a miscibility gap or solvus in the binary $CH_4 + H_2O$ system. We can use the binary system to illustrate the types of inclusions that will be produced during our experiments in the more complicated $CH_4 + H_2O$ + NaCl system.

For any combination of experimental temperature, pressure, and bulk composition that lies in the one-phase field, or outside of the solvus, the fluids contained in all inclusions have the same composition. This is illustrated by point A in Figure 3 in which fluid inclusions are formed at $T = T_{f1}$ (T_f denotes temperature of formation), and these inclusions all have a composition equivalent to point A. On cooling, these fluid inclusions enter the two-phase field at point T_HA (T_H denotes the homogenization temperature). Consequently, when viewed through a microscope at room temperature (i.e., $T \approx 22$°C), these fluid inclusions contain a CH_4-rich vapor bubble surrounded by an H_2O-rich liquid, and all inclusions have the same liquid-to-vapor ratio (Fig. 4A). Heating these inclusions results in homogenization to a single phase at some temperature that is less than the experimental temperature (e.g., point T_HA in Fig. 3). In other words, if fluid inclusions yield homogenization temperatures that are less than the temperature of formation (i.e., the experimental temperature), then the inclusions were formed in the one-phase field.

Two immiscible fluids coexist for bulk compositions that lie in the two-phase field. This is illustrated in Figure 3 by a fluid at $T = T_{f2}$ with a bulk composition given by point D. In this case, the two immiscible fluids will coexist, and these two fluid phases will have compositions given by points C and B. Each of these two fluids may be trapped independently in inclusions. In other words, two sets of fluid inclusions will form: One set of inclusions will contain a fluid enriched in CH_4 (low density), and the other set of inclusions is enriched in H_2O (high density). During cooling, both of these fluid compositions will fall within the two-phase field, and, therefore, phase separation will occur in all fluid inclusions. At room temperature, the low-density, CH_4-rich inclusions contain a relatively large CH_4 vapor bubble and a small amount of H_2O liquid. The high-density, H_2O-rich inclusions have a relatively small CH_4-rich vapor bubble (Fig. 4B,C,D). Both sets of inclusions, formed from a bulk composition that lies inside the solvus, will, theoretically, homogenize at a temperature equivalent to the experimental T (i.e., T_{f2} in Fig. 3).

Addition of NaCl to the binary $CH_4 + H_2O$ system does not change the fact that a fluid in the one-phase field, when trapped as fluid inclusions, will produce a single set of inclusions that, when viewed at room temperature, will all have the same liquid-vapor ratios. Also, a fluid in the two-phase field still produces two sets of fluid inclusions, and, therefore, fluid inclusions with two different liquid-vapor ratios may form (as in the binary system; Fig. 3). However, if NaCl were present during trapping of immiscible fluids (fluid composition in the two-phase field), the NaCl would be partitioned preferentially into the H_2O-rich endmember. In some cases, the set of H_2O + NaCl-rich fluid inclusions may be sufficiently saline to form solid NaCl crystals on cooling to room temperature (Fig. 4). Consequently, in addition to homogenization temperatures that are equivalent to the experimental temperature, and the possible presence of two sets of fluid inclusions with different liquid : vapor ratios, the presence of solid NaCl also demonstrates that the inclusions were formed from fluids trapped in the two-phase field (or possibly a three-phase field). Alternatively, a single set of inclusions with homogenization temperatures that are significantly less than the experimental temperature will form from fluids in the one-phase field.

When conducting microthermometric measurements, as the temperature increases, the pressure within the fluid inclusion also increases. When the temperature within the inclusion reaches the temperature of inclusion formation (i.e., the experimental temperature), the pressure within the fluid inclusion approximates the experimental pressure (2 kbar). Internal pressures approaching 2 kbar were, in some cases, sufficient to produce decrepitation in fluid inclusions. In other cases, the same fluid inclusion was heated several times in succession, resulting in a small increase in the homogenization temperature. This observation is consistent with an increase in the volume of the fluid inclusion, i.e., stretching (Roedder, 1981; Bodnar and Bethke, 1984). Stretching, or perhaps reversible thermal expansion, may account for the observations that some fluid inclusions may have homogenization temperatures that are slightly greater than the experimental temperature (Schmidt et al., 1998). Consequently, we exercised caution when making microthermometric measurements at temperatures at or near the experimental temperature. We typically regard the initial measurement made on any particular sample as the most reliable, particularly if subsequent measurements yield progressively higher homogenization temperatures. However, despite a few cases in which reproducible measurements were difficult to achieve due to decrepitation or stretching, in most cases, results were largely reproducible (see Table 1), generally confirming the accuracy of the microthermometric results.

4.1. Experimental Results: Extent of Immiscibility

Figure 5 shows the results of our experiments performed at 2 kbar and 300, 400, 500, and 600°C. In each diagram, the squares represent bulk compositions that lie within the one-phase field ($T_H <$ experimental T). The open circles indicate bulk compositions that were determined to lie within the two-phase field ($T_H \approx$ experimental T). The filled circles also lie within the two-phase field, but the H_2O + NaCl-rich inclusions contain daughter salts at room temperature. The solvus in these diagrams must fall between the squares and the circles, but given the distribution of compositions, its location is not well constrained. Thus, the boundary between the one- and two-phase fields (shown in Fig. 5) was calculated using the equation-of-state GEOFLUIDS (Duan et al., 1992a, 1992b, 1995).

4.1.1. 300°C experiments

Most of the fluid inclusions synthesized at this temperature homogenized at ~300°C. Therefore, the bulk compositions for all these samples likely fall within the two-phase field (Fig. 5A). However, fluid inclusions contained within sample 111F homogenized over a range of temperatures from 298.5 to 300.1°C. Because some inclusions homogenized at temperature slightly less than 300°C, it is possible that this sample actually lies within the one-phase field.

The bulk composition of the fluids contained within sample 111F is essentially equivalent (agree within uncertainty) to the composition of the boundary between the one- and two-phase fields as calculated using GEOFLUIDS and as determined experimentally by Welsch (1973). Thus, there is good agreement between all of our experiments performed at 300°C and the position of the solvus as determined using GEOFLUIDS (Fig. 5A).

4.1.2. 400°C experiments

Of the 15 experiments conducted at 400°C and 2 kbars, two samples contained NaCl daughter crystals at room temperature, and, therefore, fall within the two-phase field (Fig. 5B). Five of the 15 samples yielded homogenization temperatures that were <400°C (Table 1) and, therefore, are placed in the one-phase field in Figure 5B. Homogenization temperatures for fluid inclusions from experiment 142 were affected by decrepitation and by changes in homogenization temperatures that were presumably due to stretching. Thus, although some our results are consistent with placing sample #142 in the one-phase field as shown in Figure 5B, the measurements are not definitive, and it may be possible that sample #142 falls in the two-phase field. Furthermore, a few values of homogenization temperature measured in sample 102 are below the experimental temperature of 400°C (as low as 396°C). Consequently, our mea-

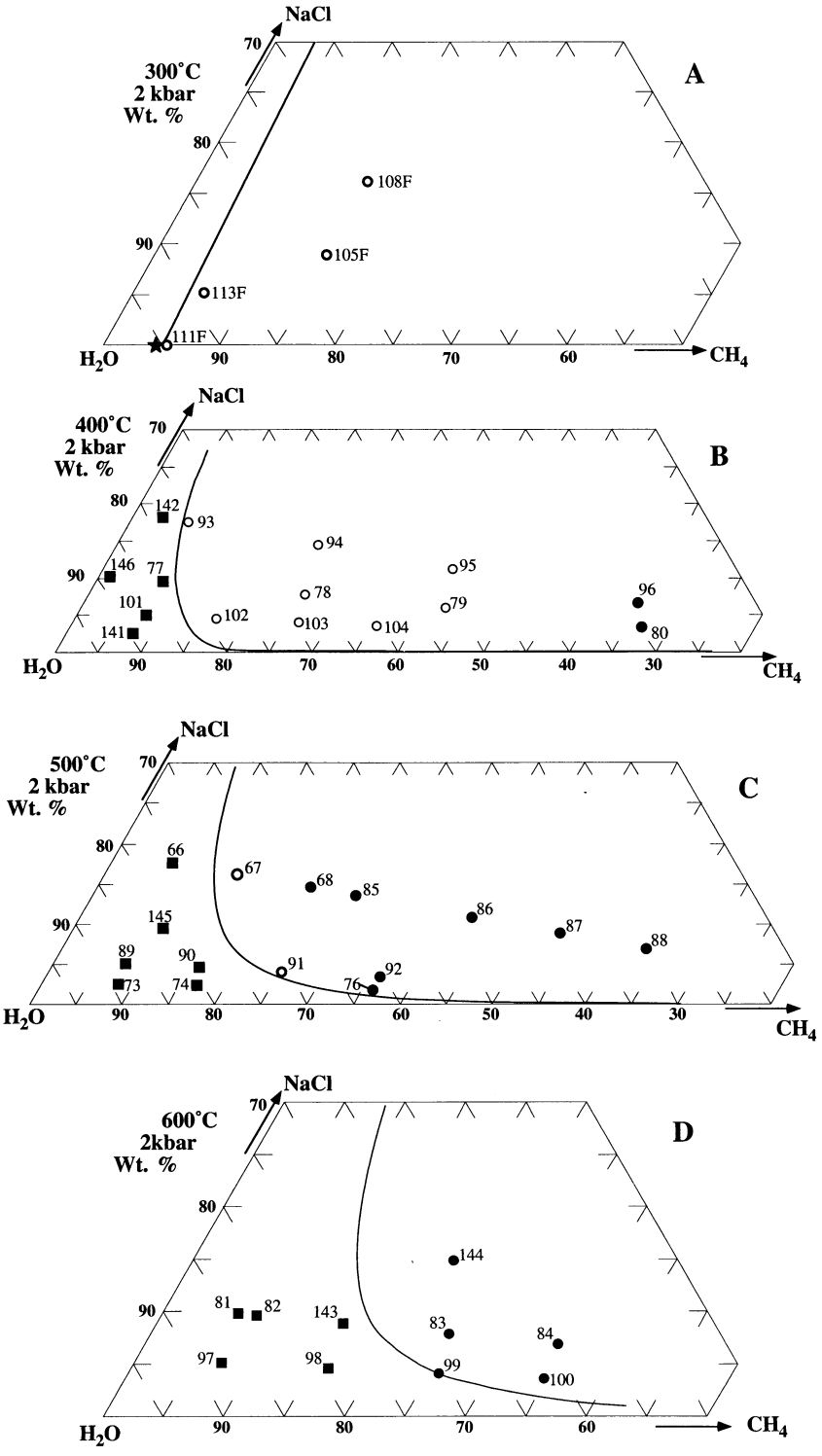

Fig. 5. Results of experiments performed at 2 kbar and 300°C (A), 400°C (B), 500°C (C), and 600°C (D). These data are contained in Table 1, and the numbers in each diagram correspond to the run numbers listed in Table 1. In each diagram, the squares represent bulk compositions that lie within the one-phase field ($T_H <$ experimental T). The open circles indicate bulk compositions that were determined to lie within the two-phase field ($T_H \approx$ experimental T). The closed circles also lie within the two-phase field; however, the H_2O+NaCl-rich inclusions produced during these experiments contain daughter salts at room temperature. The star depicted in the 300°C ternary (A) shows the location of the solvus in the CH_4-H_2O system as determined by Welsch (1973). In all diagrams, the solvus in the ternary system must lie between the circles and the squares. The location of the solvus (solid curves) was calculated using GEOFLUIDS (Duan et al., 1992a, 1992b, 1995).

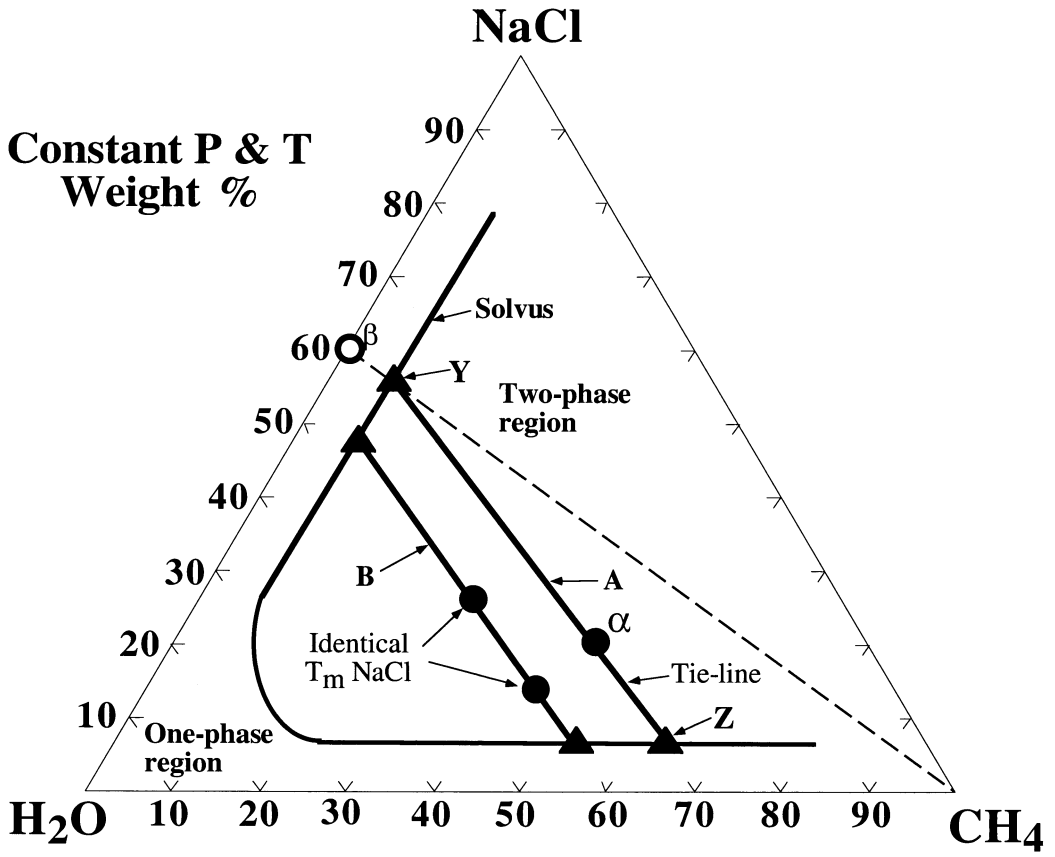

Fig. 6. Two methods for determining the compositions of co-existing immiscible fluids from the NaCl melting temperature (for both methods, the location of the solvus was calculated using GEOFLUIDS; see text). Method 1: For a fluid inclusion with bulk composition α, the aqueous phase contains 60 wt.% NaCl, as inferred from the NaCl melting temperature. Point β on the NaCl-H_2O join of the ternary diagram indicates this proportion of NaCl and H_2O. The bulk composition of this inclusion must lie along a line with a constant ratio of NaCl to H_2O (dashed line). The intersection of this line with the high-salinity portion of the solvus yields the composition of the high-density fluid (point Y). The tie-line is then constructed from this point (Y) through the bulk composition (α) to the other limb of the solvus (point Z). Method 2: Tie-lines can be located from any two samples that yield high-density inclusions with identical halite melting temperatures (T_m) and, thus, identical fluid composition. In this case, these two bulk compositions are constrained to be on the same tie-line (tie-line B).

surements for sample 102 are also not definitive and allow for the possibility that this sample falls within the one-phase field. Despite these uncertainties, all results are consistent with the location of the solvus as determined using GEOFLUIDS (Fig. 5B).

4.1.3. 500°C experiments

Six experiments performed at 500°C produced inclusions with homogenization temperatures that are significantly <500°C. Thus, the bulk compositions of the fluids in these six samples fall within the one-phase field (Fig. 5C). All other experiments performed at 500°C have bulk compositions that lie within the two- or three-phase fields. Seven experiments produced inclusions that contained NaCl daughter crystals at room temperature (Fig. 5C), whereas two samples did not contain an NaCl crystal at room temperature, yet had homogenization temperatures that were equivalent to, or in excess of, 500°C. All results are consistent with the location of the solvus as determined using GEOFLUIDS (Fig. 5C).

The fluid inclusions in sample #88 homogenized to a liquid at a temperature >500°C. Sample #88 also contained NaCl daughter crystals that melted (dissolved) at temperatures >500°C. Although we have not completely eliminated the possibility that these inclusions leaked during heating, NaCl melting temperatures >500°C suggest that the bulk composition of sample #88 lies within the three-phase field.

4.1.4. 600°C experiments

All of the experiments with bulk compositions that were determined to lie in the two-phase field at 600°C contained NaCl daughter crystals. Most other experiments produced fluid inclusions with homogenization temperatures significantly less than 600°C and, therefore, the bulk fluid composition for these experiments lies in the one-phase field.

In one case, experiment 143, efforts to measure homogenization temperatures accurately were problematic due to (1) decrepitation and (2) the fact that the fluid inclusions homogenized to the vapor phase. Previous experience (Lamb et al.,

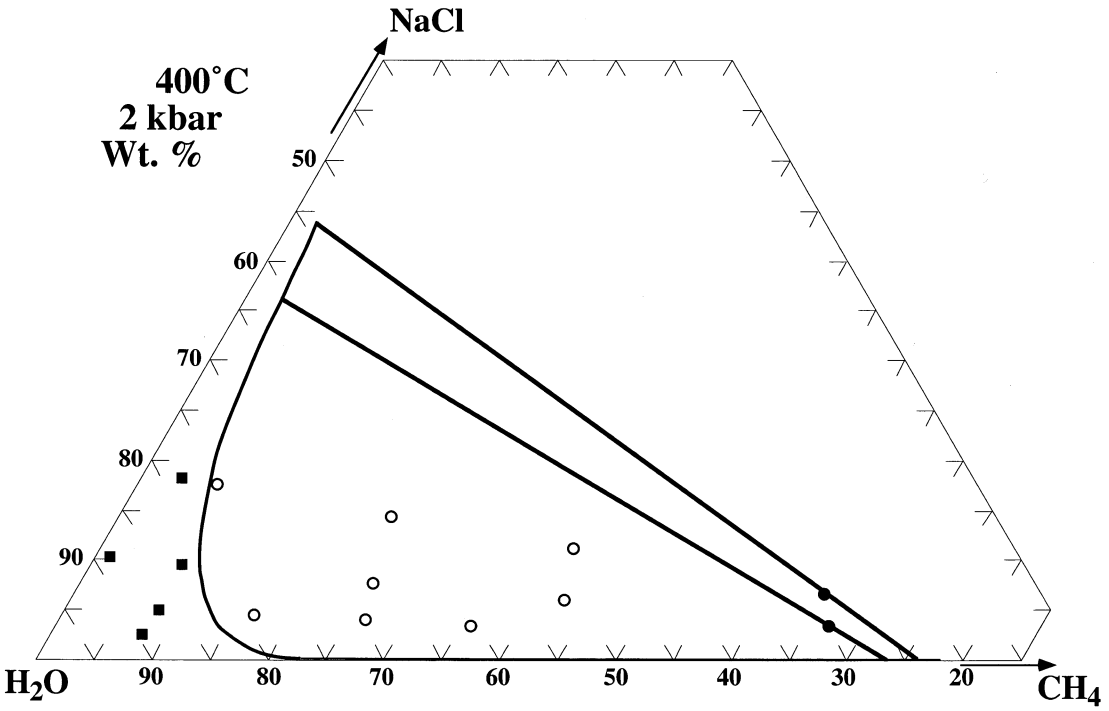

Fig. 7. Results of experiments performed at 2 kbar and 400°C. The squares represent bulk compositions that lie within the one-phase field. The circles indicate bulk compositions that were determined to lie within the two-phase field (see Fig. 5). The location of the solvus was calculated using GEOFLUIDS. Tie-lines were constructed based on salinities inferred from the melting temperatures of the NaCl (method 1; see Fig. 6 and text).

1996; this study) indicates that during trapping of immiscible fluids, the vast majority of the fluid inclusions that form contain H_2O + NaCl-rich fluids, and only a few inclusions contain CH_4-rich inclusions. In our experience, this observation holds even if application of the lever rule indicates that, during the inclusion-forming experiment, the amount of the CH_4-rich fluid is significantly greater than that of the H_2O-rich fluid. Consequently, if trapping of fluid inclusions occurs in the two-phase field, most inclusions will homogenize to a liquid. Because the fluid inclusions formed during experiment 143 homogenize to a vapor, the bulk composition of the fluid in this sample likely falls in the one-phase field. Therefore, all samples are consistent with the location of the solvus as determined using GEOFLUIDS (Fig. 5D).

5. LOCATION OF TIE-LINES IN THE TWO-PHASE FIELD

In cases where the H_2O + NaCl-rich set of inclusions contain NaCl daughter crystals at room temperature, the NaCl melting temperatures can be used to infer the ratio of NaCl to H_2O contained in the inclusions (Sterner et al., 1988). Implicit in this conclusion is the assumption that the CH_4 in these high-density inclusions has a negligible effect on the NaCl melting temperature (Lamb et al., 1996). This assumption is supported by the observation that NaCl melting occurs in the presence of a vapor bubble; thus, much of the CH_4 was partitioned into the vapor phase, whereas salt melting occurred in the H_2O-rich liquid phase. The two methods outlined below were used to determine the compositions of coexisting immiscible fluids from the NaCl melting temperature. These two methods are illustrated in Figure 6.

5.1. Method 1

To determine the location of tie-lines in the ternary system, we begin by constructing a line with a constant ratio of NaCl to H_2O. For example, point β on the NaCl-H_2O join of the ternary diagram (Fig. 6) represents a composition of 60 wt.% NaCl, 40 wt.% H_2O. The bulk composition of an inclusion with 60 wt.% NaCl, as inferred from the NaCl melting temperature, must lie along a line from point β to the corner of the ternary that corresponds to pure CH_4 (dashed line). Along this line, the ratio of NaCl to H_2O is constant, but the CH_4 content varies. The intersection of this line with the high-salinity portion of the solvus yields the composition of the high-density fluid (point Y). The tie-line is then constructed from this point (Y) through the bulk composition (α) to the low-salinity limb of the solvus (point Z). It should be noted, therefore, that the location of the tie-line depends on the location of the solvus.

5.2. Method 2

Alternatively, tie-lines can be located from any two samples formed at the same pressure and temperature with different bulk compositions that yield high-density inclusions with identical halite melting temperatures and, thus, identical fluid composition. In this case, these two bulk compositions are constrained to be on the same tie-line (tie-line B, Fig. 6).

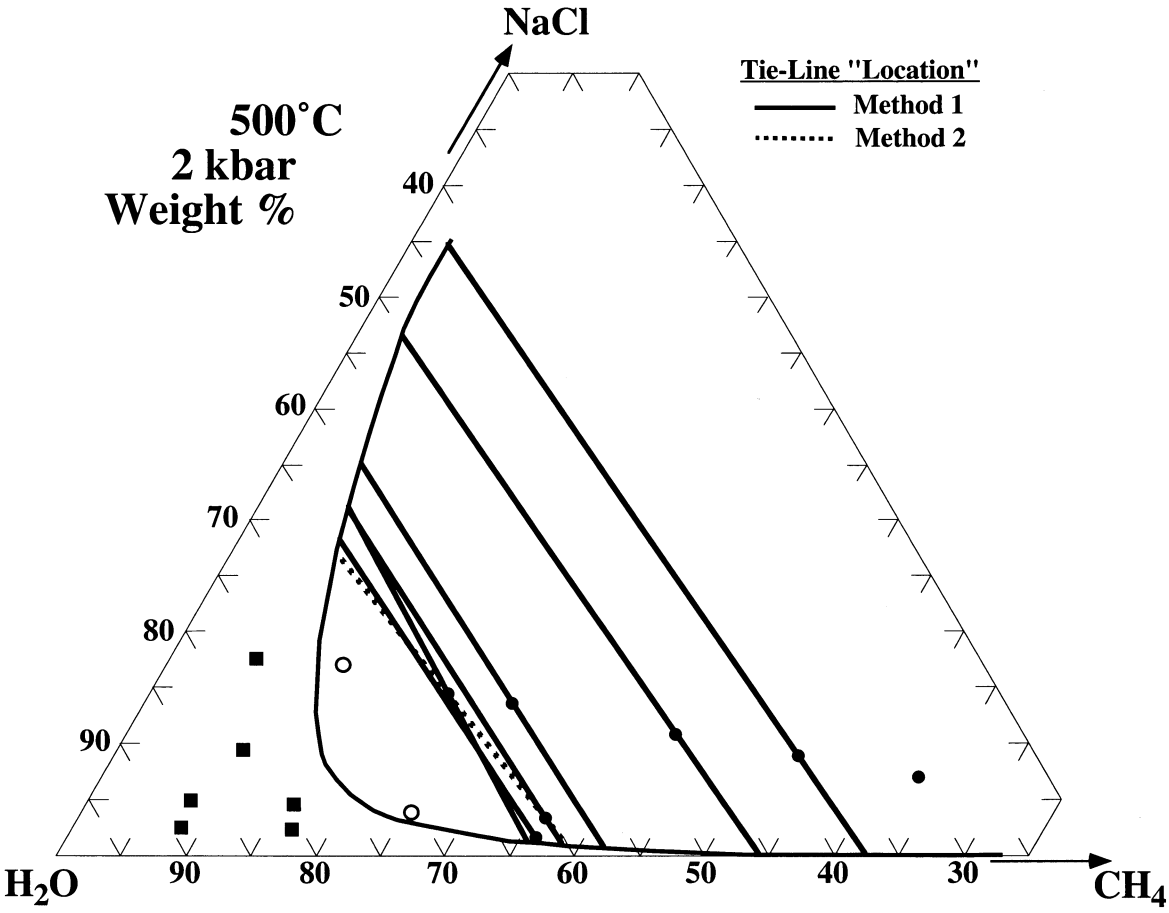

Fig. 8. Results of experiments performed at 2 kbar and 500°C. The symbols and construction of the solvus and tie-lines are the same as described for Fig. 7, except one tie-line was constructed using method 2 (dashed line). For a description of these two methods used in tie-line construction, see Fig. 6 and text.

5.3. Experimental Results: Tie-Lines

The NaCl melting temperatures (Table 1) were used to plot tie-lines in the ternary diagrams for experiments performed at 400, 500, and 600°C and 2 kbar (Figs. 7, 8, 9). In all cases, a small range in NaCl melting temperatures exists for fluid inclusions from a single sample (Table 1). One potential source of this scatter in values of NaCl melting temperatures is the possibility that the fluid inclusions did not exclusively trap one of the two endmember fluids. Any mixing of the two immiscible fluids within a single fluid inclusion would lower the salinity and, therefore, lower the melting temperature of NaCl. Thus, we chose the highest value of the melting temperature when determining the salinity of the high-density (H_2O + NaCl-rich) fluid. However, the measured range of NaCl melting temperatures in any sample is relatively small, such that use of the average melting temperature rather than the highest value for the melting temperature makes no significant difference in the phase diagrams presented below.

5.3.1. 300 and 400°C experiments

The bulk compositions of the fluids contained in all the experiments at 300°C fall within the two-phase field (Fig. 5). However, none of the inclusions contained daughter salts at room temperature and, therefore, no tie lines were constructed.

Of the 15 experiments performed at 400°C, only two experiments produced fluid inclusions that contained NaCl daughter crystals at room temperature. Thus, two tie-lines were constructed using method 1 described above (Fig. 7).

5.3.2. 500°C experiments

Seven experiments performed at 500°C produced inclusions that contained NaCl daughter crystals at room temperature. Tie-lines were constructed using method 1. Daughter crystals in samples #68 and #92 had similar melting temperatures (see Table 1) and, therefore, should lie on the same tie-line (method 2 described above). Small differences are apparent in the position ("slope") of tie-lines generated using the two different methods to locate tie-lines (Fig. 8). Although these differences are small, and are largely within the uncertainty of these two methods, the difference in the slope of the tie-lines constructed using two different methods is worthy of further discussion. The location of tie-lines using method 1 is not only a function of the NaCl content of the fluids trapped in the high-density fluid inclusions, but also the location of the solvus. The location

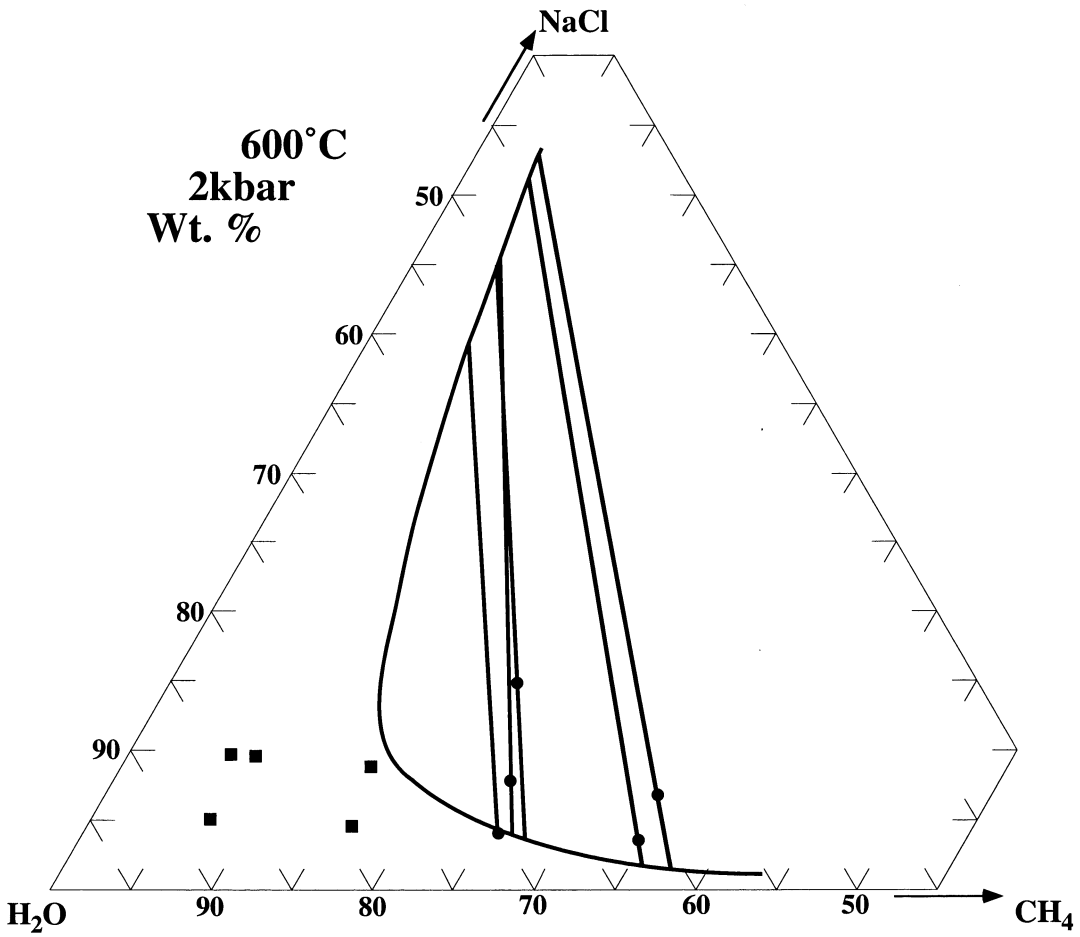

Fig. 9. Results of experiments performed at 2 kbar and 600°C. The symbols and construction of the solvus and tie-lines are the same as described for Fig. 7.

of tie-lines using method 2 (described previously) is based solely on the NaCl melting temperature. Thus, method 2 should provide the most accurate approach to tie-line location. Furthermore, the difference in the slope of the tie-lines in Figure 8, as determined using these two different methods, may simply be due to uncertainty in the location of the solvus. For example, increased consistency between methods 1 and 2 would result if the two-phase region were expanded at the expense of the one-phase region. It is possible to expand the two-phase region significantly while retaining agreement between our experiments and the location of this solvus.

5.3.3. 600°C experiments

All of the samples with bulk compositions determined to lie in the two-phase field at 600°C contained NaCl daughter crystals (Fig. 9). We used the melting temperatures of these NaCl crystals to construct tie-lines using method 1.

6. DISCUSSION AND CONCLUSIONS

6.1. A Comparison with GEOFLUIDS

Figure 10 shows the results of our experiments performed at 2 kbar compared to the results of calculations performed using the equation-of-state GEOFLUIDS (Duan et al., 1992a, 1992b, 1995). The position of the solvus, as shown in Figure 10, is based on GEOFLUIDS and is in good agreement with our experiments. However, our experiments do not place tight constraints on this boundary between the one- and two-phase fields, particularly at high salinities.

In general, the agreement between our experimentally determined location of tie-lines and calculations based on GEOFLUIDS is good (Fig. 10). However, in some cases, significant differences in the slope of the tie-lines exist between experiments and thermodynamic model. These differences are generally most pronounced for those tie-lines that join high-density fluids that are relatively NaCl-rich with low-density fluids that are relatively CH_4-rich. Our tie-line locations are, for the most part, based on (1) the salinities of these high-density fluids, as determined from NaCl melting temperatures, and (2) the location of the solvus (based on GEOFLUIDS). The salinities of the aqueous portion of the high-density fluids are $>$30 wt.% NaCl, ranging from 30.7 to 60.7 wt.% NaCl. It may be relevant, therefore, to note that the equation of state developed by Duan et al. (1995) for the system NaCl-H_2O-CO_2 (which is, in part, the basis for GEOFLUIDS) is accurate for fluid compositions up to $\sim$30 wt.% NaCl.

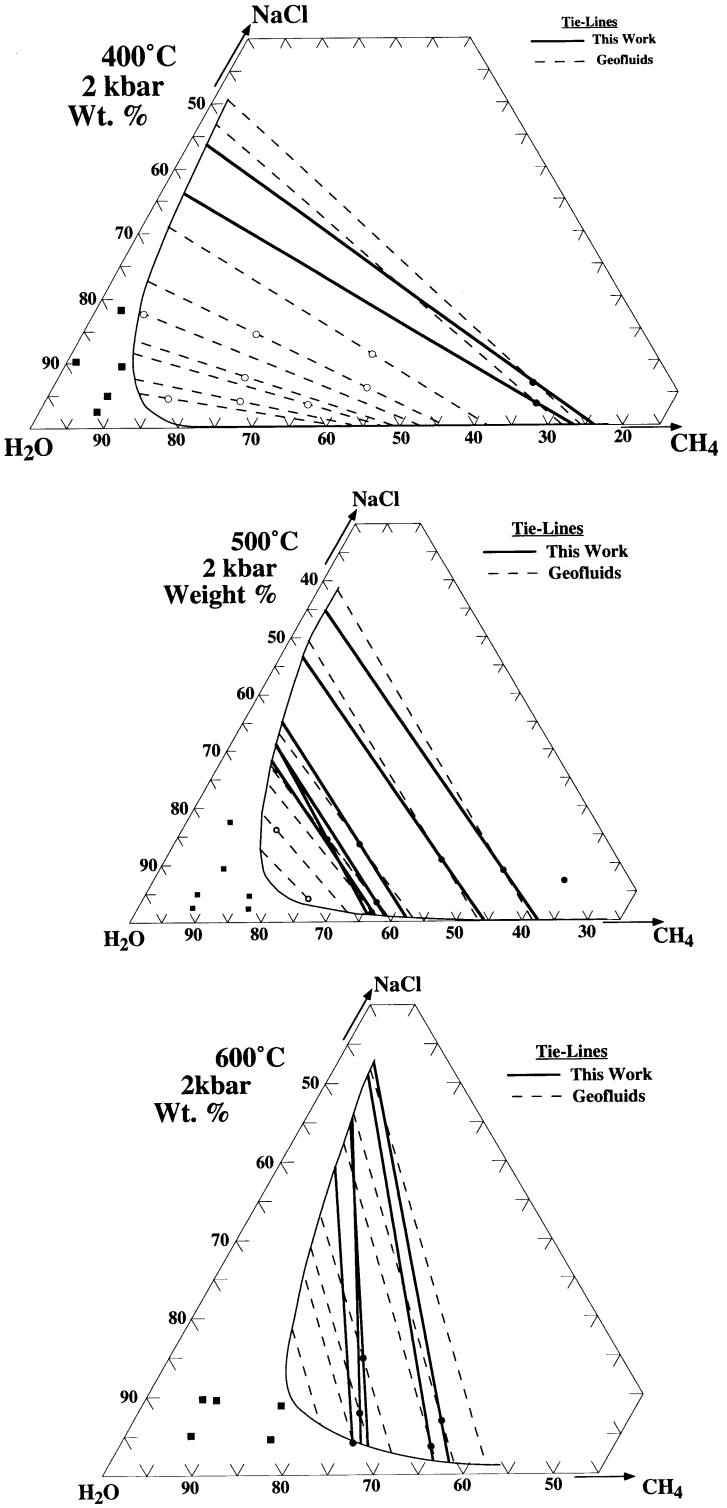

Fig. 10. Phase relations in the system CH_4-H_2O-NaCl at 2 kbar and 400, 500, and 600°C. The location of the solvus (solid curves), which is based on the equation-of-state GEOFLUIDS, is consistent with our experimental results (see text). Tie-lines based on our experiments are shown by solid lines, whereas tie-line locations based on GEOFLUIDS are shown by dashed lines.

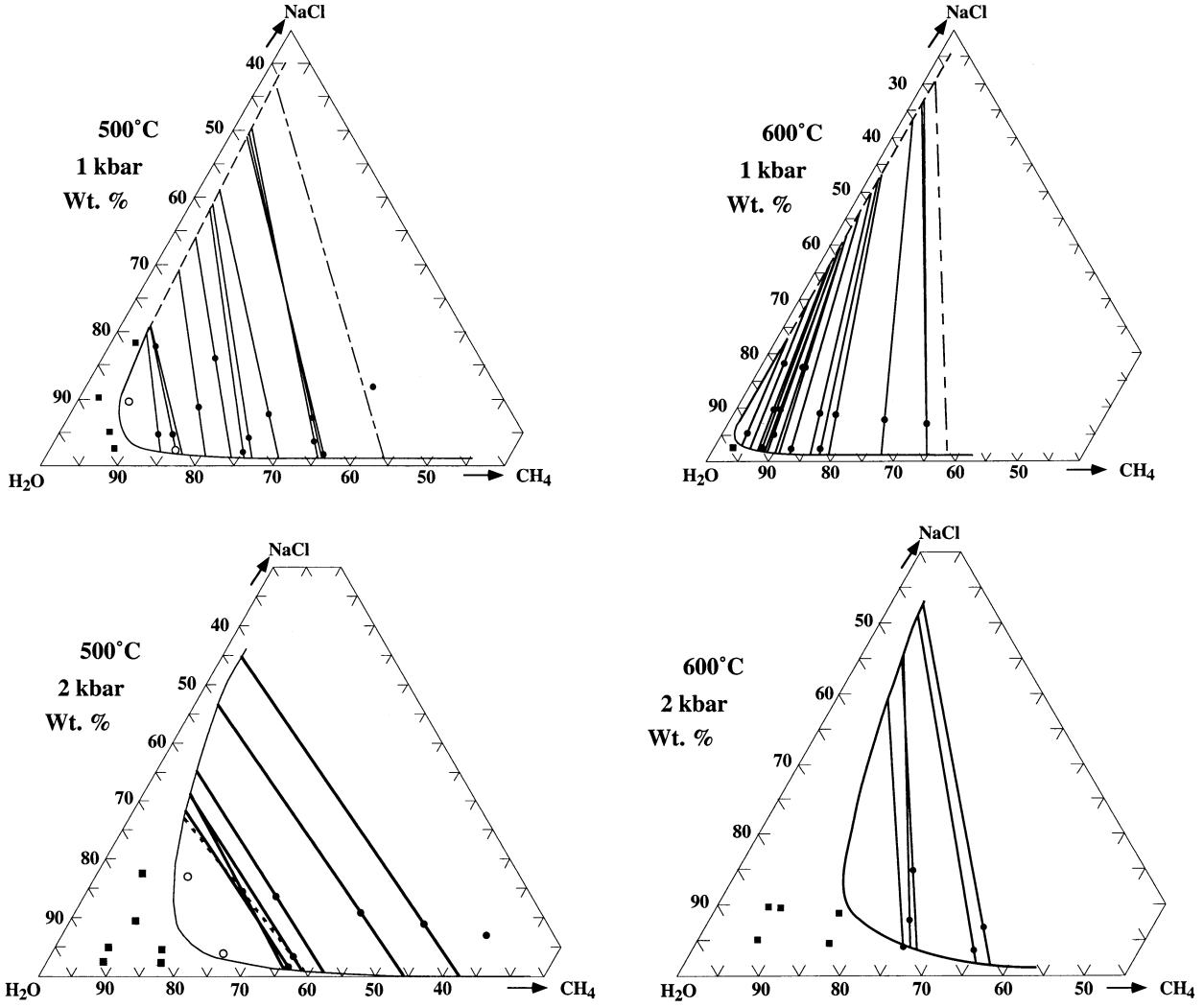

Fig. 11. Comparison of experimentally determined phase relations in the system CH_4-H_2O-NaCl at 1 kbar, 500 and 600°C (Lamb et al., 1996) and 2 kbar, 500 and 600°C (this study). At these temperatures, an increase in pressure results in a decrease in the size of the two-phase field and a change in tie-line orientation.

6.2. The Extent of Immiscibility and Tie-Line Location

The equation-of-state GEOFLUIDS predicts that the extent of immiscibility (i.e., the size of the two-phase field) will decrease with increasing temperatures in the CH_4-H_2O-NaCl system at 2 kbars. This prediction is consistent with our experimental results that clearly indicate a decrease in the size of the two-phase field with increasing temperature. We have also compared our results at 2 kbar, 500 and 600°C with the 1-kbar experiments of Lamb et al. (1996). As pressure increases from 1 to 2 kbar, the extent of immiscibility decreases at both 500 and 600°C (Fig. 11).

As temperature increases from 400 to 600°C, the slopes of tie-lines also increase (i.e., the liquid becomes more saline relative to the vapor). This change in tie-line orientation occurs at both 2 kbar (Fig. 10) and at 1 kbar (Lamb et al., 1996). As pressure increases from 1 to 2 kbar at 500 and 600°C, the slopes of tie-lines decrease (i.e., the liquid becomes less saline relative to the vapor; Fig. 11). Thus, temperature and pressure have opposite effects on tie-line orientation.

Acknowledgments—We dedicate this paper to the memory of our friend and colleague, Chris McShane, and thank Bryan Conlan for his assistance in the laboratory. We thank Robert Bodnar, Jean Dubessy, and an anonymous reviewer for constructive comments that improved the presentation of our results. This work was supported by the National Science Foundation (EAR 9117731 and EAR 9405629).

Associate editor: R. C. Burruss

REFERENCES

Bodnar R. J. and Bethke P. M. (1984) Systematics of stretching of fluid inclusions I: Fluorite and sphalerite at 1 atmosphere confining pressure. *Econ. Geol.* **79,** 141–161.

Bodnar R. J. and Sterner S. M. (1985) Synthetic fluid inclusions in natural quartz. II. Application to PVT studies. *Geochim. Cosmochim. Acta* **49,** 1855–1859.

Bodnar R. J., Burnham C. W., and Sterner S. M. (1985) Synthetic fluid inclusions in natural quartz. III. Determination of phase equilibria properties in the system H_2O-NaCl to 1000°C and 1500 bars. *Geochim. Cosmochim. Acta* **49,** 1861–1873.

Brown P. E. and Lamb W. M. (1989) P-V-T properties of fluids in the system $H_2O \pm CO_2 \pm$ NaCl: New graphical presentations and implications for fluid inclusion studies. *Geochim. Cosmochim. Acta* **53,** 1209–1221.

Carroll M. R. and Holloway J. R. (1994) Volatiles in Magmas. In *Reviews in Mineralogy*, Vol. 30 (ed. P. H. Ribbe), pp. 517. Mineralogical Society of America, Washington, D.C.

Crawford M. L. (1981) Fluid inclusions in metamorphic rocks - Low and medium grade. In *Short Course in Fluid Inclusions: Application to Petrology* (ed. L. S. Hollister and M. L. Crawford), Vol. 6, pp. 75-100, Mineralogical Association of Canada, Toronto.

Duan Z., Møller N., and Weare J. H. (1992a) An equation of state for CH_4, CO_2 and H_2O I, pure systems from 0 to 1000C from 0 to 8000 bar. *Geochim. Cosmochim. Acta* **56,** 2605–2617.

Duan Z., Møller N., and Weare J. H. (1992b) An equation of state for the CH_4-CO_2-H_2O system: II. Mixtures from 50 to 1000°C and 0 to 1000 bar. *Geochim. Cosmochim. Acta* **56,** 2619–2631.

Duan Z., Møller N., and Weare J. H. (1995) Equation of state for the NaCl-H_2O-CO_2 system: Prediction of phase equilibria and volumetric properties. *Geochim. Cosmochim. Acta* **59,** 2869–2882.

Emery D. and Robinson A. (1993) *Inorganic Geochemistry: Applications to Petroleum Geology*. Blackwell Scientific Publications, Oxford.

Frantz J. D., Zhang Y., Hickmott D. D., and Hoering T. C. (1989) Hydrothermal reactions involving equilibrium between minerals and mixed volatiles: 1. Techniques for experimentally loading and analyzing gases and their application to synthetic fluid incluisions. *Chem. Geol.* **76,** 57–70.

Frantz J. D., Popp R. K., and Hoering T. C. (1992) The compositional limits of fluid immiscibility in the system H_2O-NaCl-CO_2 as determined using synthetic fluid inclusions in conjunction with mass spectrometry. *Chem. Geol.* **98,** 237–255.

Hedenquist J. W. and Lowenstern J. B. (1994) The role of magmas in the formation of hydrothermal ore depostis. *Nature* **370,** 519–526.

Heinrich W. (1993) Fluid infiltration through metachert layers at the contact aureole of the Bufa del Diente intrusion, northeast Mexico: Implications for wollastonite formation and fluid immiscibility. *Am. Mineral.* **78,** 804–818.

Hirth G. and Kohlstedt D. L. (1996) Water in the oceanic upper mantle: Implication for rheology, melt extraction and the evolution of the lithosphere. *Earth Planet. Sci. Lett.* **144,** 93–108.

Kelley D. S. (1996) Methane-bearing fluids in the oceanic crust: Gabbro-hosted fluid inclusions from the southwest Indian Ridge. *J. Geophys. Res.* **97,** 9307–9322.

Kisch H. J. and van den Kerkhof A. M. (1991) CH_4-rich inclusions from quartz veins in the Valley-and Ridge province and the anthracite fields of the Pennsylvania Appalachains. *Am. Mineral.* **76,** 230–240.

Krader T. (1985) Phasengleichgewichte und kritische kurven des ternaren systems H_2O-CH_4-NaCl bis 250 MPa und 800 K. Ph.D. dissertation. Univ. Karlsruhe.

Lamb W. M. (1989) CO_2-rich fluid inclusions in granulites: Evidence for entrapment after the peak of metamorphism. *Mem. Geol. Soc. India* **11,** 101–115.

Lamb W. M. and Valley J. W. (1984) Metamorphism of reduced granulites in low-CO_2, vapor-free environment. *Nature* **312,** 56–58.

Lamb W. M. and Valley J. W. (1985) C-O-H fluid calculations and granulite genesis. In *The Deep Proterozoic Crust in the North Atlantic Provinces* (ed. A. Tobi and J. Touret), pp. 119–131, Reidel Pub.

Lamb W. M., Valley J. W., and Brown P. E. (1987) Post-metamorphic CO_2-rich fluid inclusions in granulites. *Contrib. Mineral. Petr.* **96,** 485–495.

Lamb W. M., Popp R. K., and Boockoff L. A. (1996) The determination of phase relations in the CH_4-H_2O-NaCl system at 1 kbar, 400 to 600°C using synthetic fluid inclusions. *Geochim. Cosmochim. Acta* **60,** 1885–1897.

Larsen R. B., Brooks C. K., and Bird D. K. (1992) Methane-bearing, aqueous, saline solutions in the Skaergaard intrusion, east Greenland. *Contrib. Mineral. Petr.* **112,** 428–437.

Mullis J., Dubessy J., Poty B., and O'Neil J. (1994) Fluid regimes during late stages of a continental collision: Physical, chemical, and stable isotope measurements of fluid inclusions in fissure quartz from a geotraverse through the Central Alps, Switzerland. *Geochim. Cosmochim. Acta* **58,** 2239–2267.

Roedder E. (1972) Composition of Fluid Inclusions. *United States Geological Survey Professional Paper*., 44JJ.

Roedder E. (1979) Fluid inclusions as samples of ore fluids. In *Geochemistry of Hydrothermal Ore Deposits* (ed. H. Barnes), pp. 684–737, Wiley-Interscience, New York.

Roedder E. (1981) Origin of fluid inclusions and changes that occur after trapping. In *Short Course in Fluid Inclusions: Applications to Petrology* (ed. L. S. Hollister and M. L. Crawford), Vol. 6, pp. 101–137.

Roedder E. (1984) *Fluid inclusions*. Reviews in Mineralogy, v. 12, Mineralogical Society of America, Washington, D.C.

Schmidt C. and Bodnar R. J. (2000) Synthetic fluid inclusions: XVI. PVTX properties in the system H_2O-NaCl-CO_2 at elevated temperatures, pressures, and salinities. *Geochim. Cosmochim. Acta* **64,** 3853–3869.

Schmidt C., Rosso K. M., and Bodnar R. J. (1995) Synthetic fluid inclusions: XIII. Experimental determination of PVT properties in the system H_2O + 40 wt% NaCl + 5 mole% CO_2 at elevated temperature and pressure. *Geochim. Cosmochim. Acta* **59,** 3953–3959.

Schmidt C., Chou I.-M., Bodnar R. J., and Bassett W. A. (1998) Microthermometric analysis of synthetic fluid inclusions in the hydrothermal diamond-anvil cell. *Am. Mineral.* **83,** 995–1007.

Shelton K. L. and Orville P. M. (1980) Formation of synthetic fluid inclusions in natural quartz. *Am. Mineral.* **65,** 1233–1236.

Sterner M. S. and Bodnar R. J. (1991) Synthetic fluid inclusions. X. Experimental determination of the P-V-T-X properties in the CO_2-H_2O system to 6 kb and 700°C. *Am. J. Sci.* **291,** 1–54.

Sterner M. S., Hall D. L., and Bodnar R. J. (1988) Synthetic fluid inclusions. V. Solubility relations in the system NaCl-KCl-H_2O under vapor saturated conditions. *Geochim. Cosmochim. Acta* **52,** 989–1006.

Welsch H. (1973) Die Systeme Xenon-Wasser und Methan-Wasser bei hohen Drucken und Temperaturen. Ph.D. dissertation. Karlsruhe.

Zhang Y. and Frantz J. D. (1987) Determination of the homogenization temperatures and densities of supercritical fluids in the system NaCl-KCl-$CaCl_2$-H_2O using synthetic fluid inclusions. *Chem. Geol.* **64,** 335–350.

Zhang Y. and Frantz J. D. (1992) Hydrothermal reactions involving equilibrium between minerals and mixed volatiles: 2. Investigations of fluid properties in the CO_2-CH_4-H_2O system using synthetic fluid inclusions. *Chem. Geol.* **100,** 51–72.